CHEMISTRY OF MATERIALS

pubs.acs.org/cm

Article

Zwitterionic Ion-Selective Membranes with Tunable Subnanometer Pores and Excellent Fouling Resistance

Samuel J. Lounder and Ayse Asatekin*

Cite This: *Chem. Mater.* 2021, 33, 4408−4416

Read Online

ACCESS | Metrics & More | Article Recommendations | Supporting Information

ABSTRACT: Nanofiltration (NF) membranes are an energy-efficient, scalable technology for water treatment and reuse. However, they are prone to fouling and offer limited selectivity between ions, hampering their use in water recovery and reuse. This work utilizes scalable self-assembly of zwitterionic copolymers combined with a novel cross-linking approach to develop membranes distinguished by exceptional mono/divalent ion selectivity, tunable pore size, and complete resistance to irreversible fouling. Extended cross-linking reduces the pore size to ∼0.9 nm, the smallest pore size reported for self-assembled copolymer membranes to date. These membranes achieve >99.2% SO_4^{2-} rejection and a Cl^-/SO_4^{2-} selectivity of 101, demonstrating their promise for energy-efficient sulfate removal and other water treatment applications.

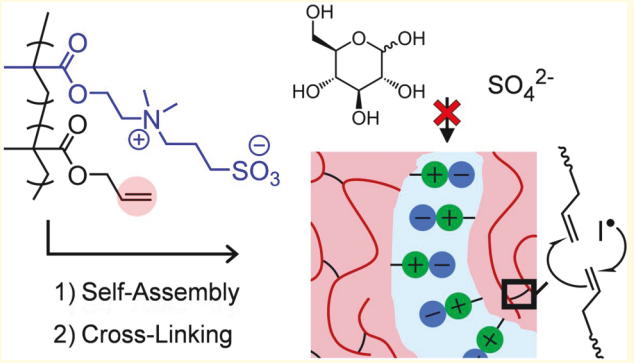

INTRODUCTION

Sustainable technologies that separate salt(s) from water are urgently needed to address global water scarcity as well as energy-intensive water treatment processes for industrial use. Membrane filtration is an energy-efficient, small-footprint water treatment technology.[1] Reverse osmosis (RO) membranes are designed for water desalination,[1−3] whereas nanofiltration (NF) membranes enable lower pressure removal of divalent ions for facile water reuse and scaling prevention.[4] However, there is an urgent need for RO/NF membranes with improved selectivity and fouling resistance.[1,5−7] Many industrial water recovery and reuse applications require selective removal of divalent ions (e.g., Ca^{2+}, SO_4^{2-}) while allowing the passage of NaCl. Current NF membranes still exhibit significant NaCl retention, requiring higher pressures to overcome the osmotic pressure difference. Fouling management in water softening and desalination involves added process steps, leading to increased process complexity, cost, and energy use.

Progress in the development of better RO/NF membranes has been curtailed by the narrow portfolio of available materials. Polyamide thin film composite membranes (PA-TFCs) have remained the predominant RO/NF technology since their conception about four decades ago.[2,8] Thin film nanocomposites (TFNs), defined as PA-TFCs that incorporate nanoscale constituents (e.g., functionalized carbon nanotubes,[9] graphene oxide,[10] MOFs,[11] and polymeric nanoparticles[12]), exhibit improved performance, but polyamide chemistry makes it difficult to accurately control selectivity, achieve chlorine resistance, and prevent fouling. Novel materials that address selectivity and fouling resistance by design are required to overcome these limitations.[8,13]

Self-assembly is a powerful tool for fabricating nanostructured membranes with uniform pore size, controlled surface/pore chemistry, and exceptional performance.[13,14] Membranes prepared from polymerized lyotropic liquid crystals (LLCs), for example, possess subnanometer transport channels that retain mono- and divalent ions.[15,16] Block copolymer (BCP) self-assembly has been used to manufacture ultrafiltration (UF) membranes possessing monodisperse pores with controlled functionality[8,13,17−21] but low ion retention due to relatively large pores. To reduce the BCP membrane pore size into the NF regime,[19] researchers utilized block(s) that swell into the pore upon postfunctionalization.[17−21] This enabled charge-based separations for ∼1 nm molecules[17] or ∼2 nm pores that remained stable over a broad pH range.[20] However, these approaches have not led to appreciable ion selectivity.

Random zwitterionic amphiphilic copolymers (r-ZACs) are random/statistical copolymers of zwitterionic and hydrophobic monomers. Strong zwitterion−zwitterion interactions drive microphase separation into bicontinuous networks of zwitter-

Received: February 1, 2021
Revised: May 21, 2021
Published: June 4, 2021

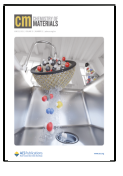

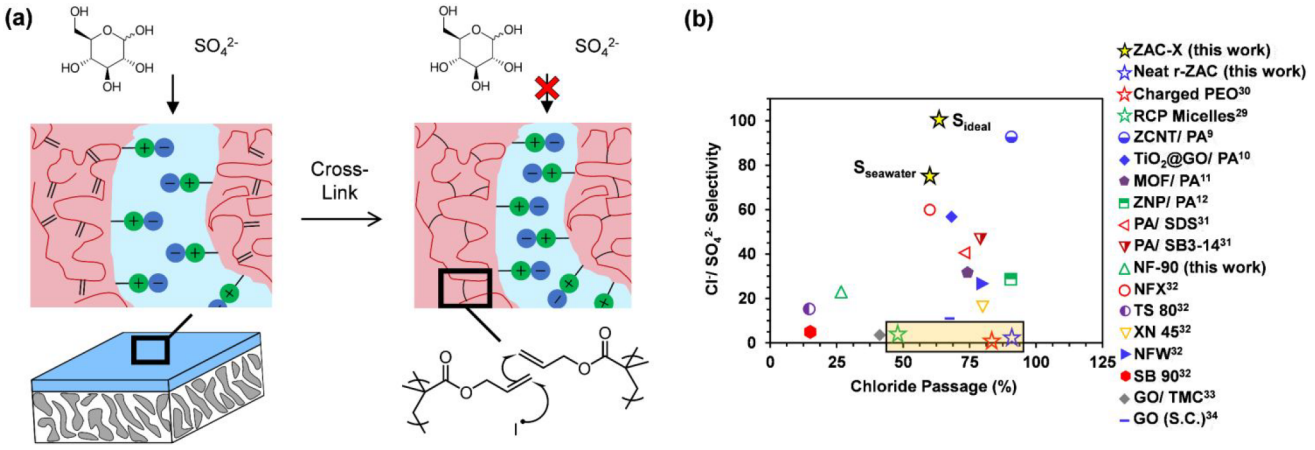

Figure 1. (a) Schematic showing a cross-linkable r-ZAC TFC membrane and the tuning of its selectivity. Red pore walls represent the hydrophobic/cross-linkable domains, while blue channels represent the hydrophilic/zwitterionic domains through which water and small solutes permeate. Selectivity is tuned by cross-linking the hydrophobic domain through allylic double bonds, arresting the zwitterionic nanochannels in a state of limited swelling. This reduces the pore size and enables the rejection of subnanometer solutes. (b) Performance comparison of highly cross-linked r-ZAC membranes (ZAC-X) against state-of-the-art membranes featuring nanostructured copolymer selective layers (star symbols, marked with gold region),[29,30] polyamide TFNs,[9−12] polyamide TFCs,[31,32] and inorganic selective layers.[33,34] ZAC-X demonstrated exceptional Cl^-/SO_4^{2-} selectivity, surpassing the performance of other membrane technologies even when challenged with artificial seawater.

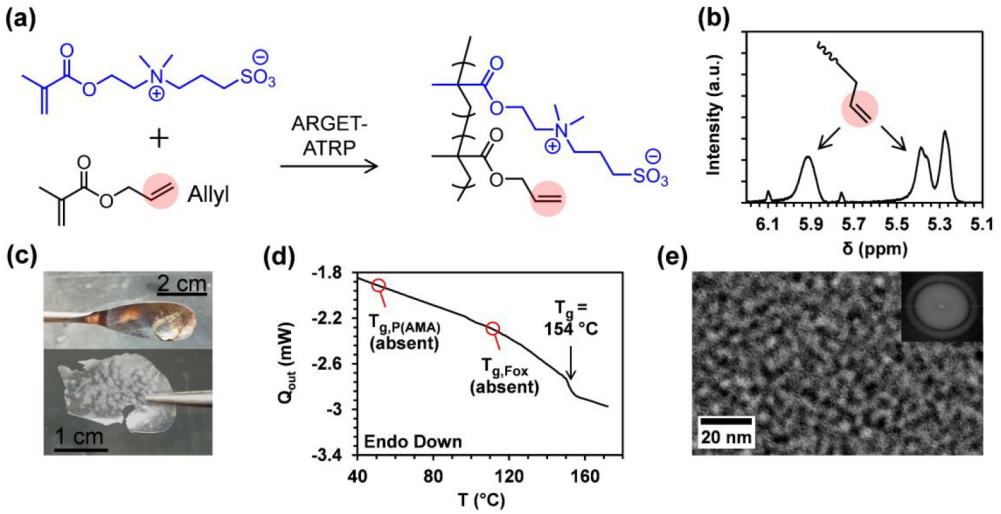

Figure 2. (a) Synthesis scheme for P(AMA-*r*-SBMA) via ARGET-ATRP. (b) Copolymer ^{1}H NMR spectra for 6.2−5.1 ppm (500 MHz, d_6-DMSO), showing broad allyl peaks indicating the preservation of AMA units. (c) (Top) Photograph of the gel formed by exposing a solution of copolymer (3 wt %) and photoinitiator (5 wt %) to UV light. (Bottom) Photograph of a cross-linked copolymer film after several weeks of immersion in TFE. No discernible change in swelling, color, or opacity was observed, whereas uncross-linked copolymer films readily dissolve in TFE. (d) DSC thermogram for uncross-linked copolymer (second run, 30 °C/min heating rate). (e) TEM bright-field image for uncross-linked copolymer showing a bicontinuous network of zwitterionic nanochannels (dark) surrounded by the hydrophobic phase (light). (Inset) FFT of the image with the dark ring corresponding to the spatial frequency of the zwitterionic domains.

ionic and hydrophobic nanodomains.[22−25] TFC membranes with r-ZAC-selective layers can be prepared by coating a thin (∼1 μm) copolymer layer onto a porous support.[22,23,26,27] During aqueous filtration, the zwitterionic domain functions as a network of hydrophilic nanochannels for the transport of water and small solutes.[22,23] Due to the strong hydration of the zwitterions, these membranes exhibit unprecedented fouling resistance, fully retaining their permeability during the filtration of real and simulated wastewater streams containing high concentrations of oil and biomacromolecules.[22,23,27,28] This makes r-ZAC membranes extremely promising for treating feeds such as challenging wastewater streams or littoral seawater.

These membranes remove larger organic compounds (>1000 Da) and exhibit low retention of mono/divalent ions, corresponding to size-based selectivity with a size cutoff of ∼1.5 nm.[22,23,26,27] However, past efforts aimed at tuning the pore size of r-ZACs through the manipulation of hydrophobic and zwitterionic monomer chemistry have not been successful. Changing the hydrophobic group chemistry,[22] zwitterionic group chemistry,[23] or monomer ratios[22] led to minimal changes in their microphase-separated domain sizes and effective pore size. Tuning the effective pore size of r-ZAC-based membranes down to <1.0 nm would enable their use in novel applications such as ion separations and the removal of small organic compounds (e.g., pharmaceuticals, endocrine disruptors).

https://doi.org/10.1021/acs.chemmater.1c00374
Chem. Mater. 2021, 33, 4408−4416

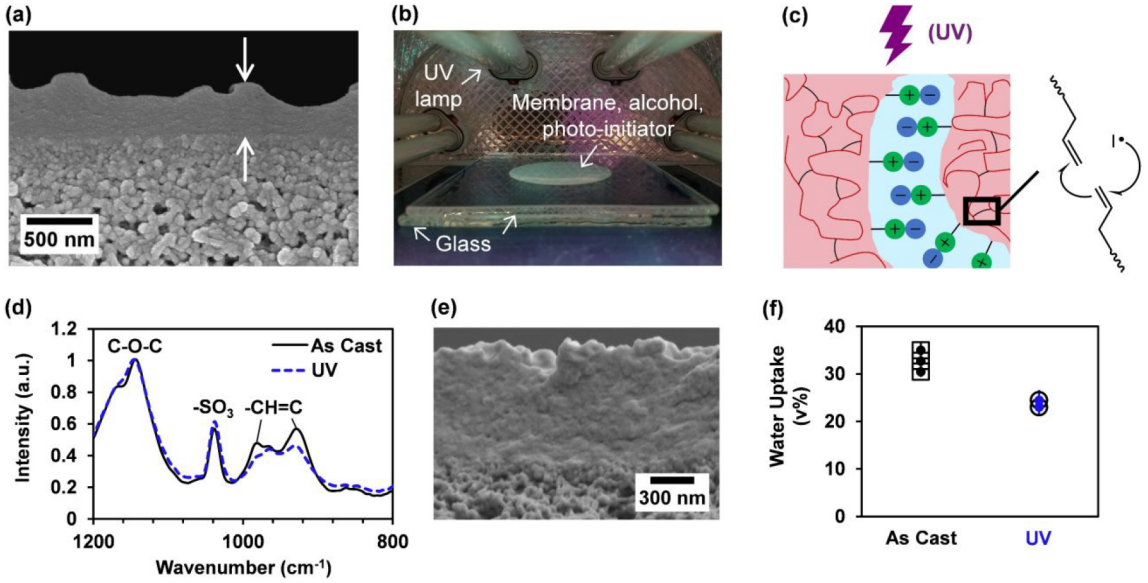

Figure 3. (a) Cross-sectional field emission scanning electron microscope (FESEM) image of TFC membranes featuring an ~300−500 nm P(AMA-*r*-SBMA) selective layer covering the support. (b) Diagram showing a membrane disk prepared for cross-linking. (c) Schematic showing cross-linking of the hydrophobic domains of P(AMA-*r*-SBMA) via photopolymerization. (d) ATR-FTIR spectra of as-cast and cross-linked films of P(AMA-*r*-SBMA) (20 min UV cure with 3.0 w/v % photoinitiator). (e) Cross-sectional SEM image of a cross-linked TFC membrane that was immersed in TFE, a good solvent for P(AMA-*r*-SBMA), for several weeks. The selective layer did not dissolve, confirming that it was cross-linked. (f) Water uptake for uncross-linked (as cast) and cross-linked (UV, 5 min cure time, 3.0 w/v % photoinitiator) films of P(AMA-*r*-SBMA).

In this work, we present self-assembled TFC membranes distinguished by tunable subnanometer pore size, exceptional ion selectivity, and complete resistance to irreversible fouling. These membranes feature an r-ZAC-selective layer with a cross-linkable hydrophobic phase, providing a new and scalable route for precisely reducing the self-assembled pore size (Figure 1a). This approach allows selectivity to be easily tuned for desired applications, ranging from the removal of large organics to sulfate removal and water softening. For instance, selective removal of SO_4^{2-} ions from saline streams is crucial for various oil and natural gas extraction processes, industrial water and wastewater treatment, and treating groundwater sources that are high in sulfate. The most highly cross-linked membranes feature the smallest nanochannels ever reported for a self-assembled copolymer membrane and achieve one of the highest Cl^-/SO_4^{2-} selectivities reported for any filtration membrane (Figure 1b). The strongly hydrated zwitterionic groups also impart exceptional fouling resistance to both natural organic matter and proteins. These critical features, combined with high water permeance and tunable selectivity, enable this novel membrane family to address various separations, from water recovery and industrial reuse to the treatment of high-organic-content wastewater streams.

RESULTS AND DISCUSSION

Cross-Linkable r-ZAC Synthesis and Characterization.

We synthesized the cross-linkable r-ZAC by copolymerizing cross-linkable allyl methacrylate (AMA) and zwitterionic sulfobetaine methacrylate (SBMA) via activators regenerated by electron transfer atom transfer radical polymerization (ARGET-ATRP) (Figure 2a, Figure S2). AMA contains two reactive sites, but the methacrylic double bonds are more reactive than the allylic double bonds.[35] Most allyl groups are preserved when using a controlled radical polymerization technique such as ARGET-ATRP,[35−37] particularly when the reaction conditions are selected carefully, i.e., ambient temperature,[35] low conversion,[35] and low monomer concentration.[36] Using this approach, we obtained linear r-ZACs with extensive allyl functionality (Figure 2b). The copolymer composition (53 wt % AMA) closely matched that of the reaction mixture (60 wt % AMA) at ~10% conversion, suggesting a near-random repeat unit sequence. Despite this low conversion and the mild reaction conditions that were employed, the copolymer chains were reasonably large (45−60 nm, corresponding to 2.0×10^6−2.6×10^6 g/mol based on polyacrylonitrile standards in dimethylformamide) based on dynamic light scattering (DLS) measurements (Table S2). Peak integration of the ^{1}H NMR spectra indicates that essentially every allyl group was preserved, corroborated by the absence of gel formation during the synthesis.

The abundant allyl groups enabled facile cross-linking by UV-initiated photopolymerization (Figure 2c). In one demonstration, we formed a gel by exposing a solution of copolymer (3 wt %) and photoinitiator (5 wt %) to UV light. In another demonstration, we exposed a free-standing copolymer film equilibrated with a 3 w/v % solution of photoinitiator/isopropyl alcohol to UV light. This treatment rendered the copolymer film insoluble in trifluoroethanol (TFE), confirming cross-linking.

Microphase separation in the copolymer was confirmed by differential scanning calorimetry (DSC, Figure 2d), which showed a single glass transition temperature (T_g) of 154 °C.

No transitions were observed around the T_g of P(AMA), ~54 °C.[37] The measured T_g is significantly higher than 115 °C, the value predicted if the copolymer was a homogeneously mixed single phase using the Fox equation (eq S1). This implies that the measured T_g is associated with the zwitterion-rich domain.[23,38] This domain likely limits the mobility of the polymer segments in the bordering AMA-rich hydrophobic domain due to the high degree of interconnectivity, thereby obscuring its lower temperature glass transition.[23] This is consistent with the behavior of other r-ZACs that microphase

https://doi.org/10.1021/acs.chemmater.1c00374
Chem. Mater. 2021, 33, 4408−4416

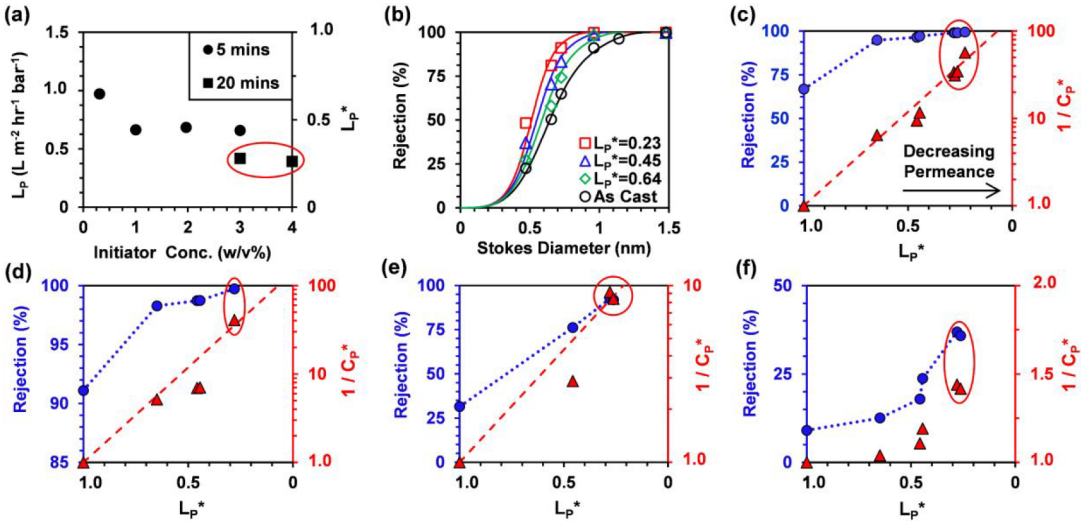

Figure 4. (a) L_P (left axis) and L_P* (right axis) versus photoinitiator concentration for different cure times. (b) Rejection of neutral solutes vs Stokes diameter for membranes cross-linked to different extents. Greater reductions in permeance resulted in progressively smaller pores. Solid lines are fits to the DSPM[46] for uniform pore diameters of 0.94, 1.06, 1.17, and 1.36 nm for L_p* = 0.23, L_p* = 0.45, L_p* = 0.64, and as cast, respectively (Table S3). (c–f) Rejection (left axis, ●) and $1/C_P$* (right axis, ▲) versus L_P* for (c) Na_2SO_4, (d) sucrose, (e) $MgCl_2$, and (f) NaCl. Rejection and $1/C_P$* increased with decreasing L_P*, indicating progressively smaller pores. Performance of the most highly cross-linked membranes selected for further study, ZAC-X, is circled in red. Pressure was 250 psi.

separate to form bicontinuous networks of ∼1−2 nm hydrophobic and zwitterion-rich domains.[22,23,38] We characterized the self-assembled morphology by transmission electron microscopy (TEM, Figure 2e). The zwitterionic domains were positively stained by immersion in 2% $CuCl_2$, resulting in the formation of sulfobetaine−copper complexes. We observed a bicontinuous network of percolated zwitterionic nanochannels (dark regions) surrounded by the hydrophobic/cross-linkable phase (light regions), consistent with previously reported r-ZACs.[23] The fast Fourier transform (FFT) of the TEM image lacked directional features (inset of Figure 2e, Figure S3a), indicating a disordered network.[23,39] To determine the average nanochannel width (D), we plotted the periodic intensity from the FFT against the reciprocal of the corresponding spatial frequency (Figure S3b). The characteristic length scale given by the outer ring of the FFT was d = 2.8 nm, corresponding to an average nanochannel width of D = 1.4 nm,[39] corresponding to the zwitterionic domain width in the dry state.

Membrane Fabrication and Cross-Linking. Uncross-linked r-ZAC TFCs, termed ZAC-0, were prepared by coating a solution of P(AMA-*r*-SBMA) in TFE onto a commercial ultrafiltration (UF) membrane as a porous support (PS35, Solecta). Resultant selective layers were ∼300−500 nm in thickness (Figure 3a). The membrane morphology was somewhat irregular, likely due to rapid solvent evaporation. The average permeance, defined as water flux normalized by operating pressure, was 1.5 L m^{-2} h^{-1} bar^{-1}. While this permeance is comparatively low for most NF membranes, our previous experiences with r-ZAC-based membranes have shown that it can be drastically enhanced by improved manufacturing methods that decrease coating thickness and enhance the interconnectivity of zwitterionic domains. For instance, the use of ionic liquid additives in the coating solutions used to make r-ZAC membranes increased the permeance by up to 50 times without loss of selectivity.[40] Electrospray coating the r-ZAC also led to significantly thinner selective layers and order-of-magnitude increases in water permeance.[41] We expect that further development of the coating process will lead to further enhanced permeances, on par with commercial membranes.

The effective pore size of ZAC-0 was estimated to be 1.36 nm based on a fit to the Donnan Steric Pore Model (see Supporting Information for the model; raw data shown in Table S3). ZAC-0 exhibited relatively low retentions of Na_2SO_4 (67%), $MgCl_2$ (32%), and NaCl (9.1%), similar to that of previously reported r-ZAC membranes[27] and in agreement with previous data indicating that the hydrophobic domain chemistry has a limited effect on the pore size.[22]

To cross-link the copolymer-selective layer and thereby tune the nanochannel diameter, ZAC-0 or equivalent P(AMA-*r*-SBMA) films were first equilibrated with a solution of photoinitiator (2-hydroxy-2-methylpropiophenone) in isopropanol (Figure 3b). UV irradiation then initiated radical polymerization of the allylic double bonds in the hydrophobic phase, cross-linking the membrane-selective layer (Figure 3c). Attenuated total reflectance Fourier transform infrared (ATR-FTIR) spectroscopy of P(AMA-*r*-SBMA) films showed a reduction in the −CH═C allyl peak[42] intensity upon curing (Figure 3d), confirming that a large fraction of the allyl groups reacted. UV curing also rendered the P(AMA-*r*-SBMA)-selective layer of TFC membranes insoluble in TFE (Figure 3e), providing further evidence for cross-linking.

Water uptake measurements indicated that cross-linking reduced the aqueous swelling of P(AMA-*r*-SBMA) films (Figure 3f). Since polar solvents such as water preferentially swell the zwitterionic domain of microphase-separated r-ZACs,[43,44] this implies that cross-linking prevents the nanochannels from expanding in water and provides a clear mechanism for pore size reduction.[45] The zwitterionic nanochannels were less swollen when equilibrated with the isopropanol/photoinitiator solution than with water. Hydrophobic plasticizers preferentially swell the hydrophobic domain of microphase-separated r-ZACs,[44] minimally penetrating the zwitterionic domain due to unfavorable interactions; SBMA and poly(SBMA) are both insoluble in isopropanol. Upon

https://doi.org/10.1021/acs.chemmater.1c00374
Chem. Mater. 2021, 33, 4408−4416

cross-linking, the membrane was trapped in this low-swelling state, reducing subsequent aqueous swelling and thus resulting in a smaller effective pore size. Higher degrees of cross-linking restrict swelling more, reducing the pore size to a greater extent. One would expect this to simultaneously reduce water flux and increase solute/water selectivity.[45] The water uptake of the cross-linked films was 24%, which is within the typical range for the selective layer of polyamide NF membranes.[45] This suggests that the cross-linked r-ZAC membranes could exhibit a similar effective pore size.

Tuning of Membrane Selectivity. To determine how cross-linking affects membrane performance, we first defined the normalized permeance (L_P*) to quantify the decrease in the water flux through the membrane upon cross-linking

$$L_P^* = \frac{L_P}{L_{P,initial}} \quad (1)$$

where L_P and $L_{P,initial}$ are the permeances of the cross-linked membrane and ZAC-0, respectively. Permeance decreased upon cross-linking, resulting in L_P* < 1 (Figure 4a). The reaction conditions that were expected to result in higher degrees of cross-linking, specifically longer cure times (5−20 min) and higher photoinitiator concentrations (0.30−4.0 w/v %), led to greater permeance decreases (Figure 4a).

To clearly demonstrate that the permeance decrease upon cross-linking leads to a tunable shift in the effective pore size, we filtered a series of neutral solutes using ZAC-0 and membranes cross-linked to varying extents (Figure 4b). The effective pore size of each membrane was fitted with a single pore diameter using the Donnan Steric Pore Model[46] (eqs S5−S10, Table S3). A lower permeance corresponded to smaller pores, with the effective pore size ranging from 1.36 nm for ZAC-0 to 0.94 nm for the most highly cross-linked membranes. This result clearly illustrates that the membrane pore size was tuned by the extent of cross-linking. Interestingly, a single pore diameter was successfully fit to each membrane, suggesting that the pore size distribution of these membranes was likely relatively narrow and that the pore shrinking process was uniform and well controlled.

To further characterize the tuning of the selectivity, we defined the inverse normalized permeate concentration ($1/C_P$*) to quantify how the selectivity between the solute and water changes upon cross-linking

$$\frac{1}{C_P^*} = \frac{C_{P,initial}}{C_P} \approx \left(\frac{J_w}{J_{solute}}\right) / \left(\frac{J_{w,initial}}{J_{solute,initial}}\right) \quad (2)$$

where C_P and $C_{P,initial}$ are permeate concentrations, J_{solute} and $J_{solute,initial}$ are solute fluxes, and J_w and $J_{w,initial}$ are water fluxes through the cross-linked membrane and ZAC-0, respectively. A high $1/C_P$* implies an enhancement in water/solute selectivity, likely due to pore size reductions.

We saw $1/C_P$* increase exponentially with decreasing L_P* for both neutral solutes (sucrose, riboflavin) and salts (Na_2SO_4, $MgCl_2$) with the full range of cross-linking conditions falling onto a single master curve for each solute (Figure 4c−e, Figure S7). This further confirms that cross-linking leads to a reduction in pore size. It also provides a useful guide for tuning the selectivity, enabling the manufacture of custom membranes for targeted applications (e.g., larger pores for dye removal; smaller pores for ion separation). $1/C_P$* increased much less for NaCl (Figure 4f), making this approach well suited for applications where monovalent ion retention is not desired. Such precise and simple tuning is not feasible with the state-of-the-art NF membrane chemistry.

Fouling Resistance of Highly Cross-Linked Membranes. Fouling is a major challenge for membrane treatment of high-organic-content streams, dominating operating costs and significantly impacting the economic and technical feasibility of membrane treatment.[22,23,27,47] Exceptional fouling resistance represents a key feature of previous r-ZAC membranes,[22,23,27] which resist foulant adsorption due to the hydrophilicity of the zwitterionic nanochannels.

To determine if this antifouling property is observed in the highly cross-linked r-ZAC membranes with subnanometer pores, we challenged the most highly cross-linked membranes, termed ZAC-X, in two fouling experiments (Figure 5). ZAC-X

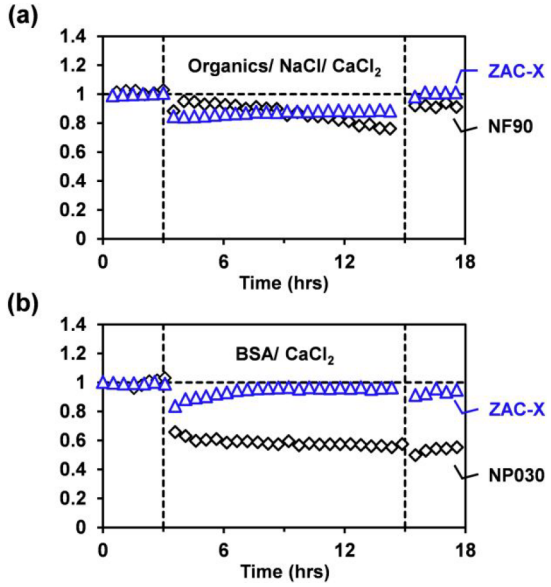

Figure 5. Fouling of highly cross-linked r-ZAC membranes (ZAC-X). y axis shows instantaneous flux (J) normalized by initial water flux (J_0). Commercial NF membranes are included as controls. (a) Fouling by a solution containing common foulants in surface water (50 ppm of humic acid, 50 ppm of sodium alginate, 1 mM $CaCl_2$, 10 mM NaCl, pH = 7, J_0 = 8.7 L m^{-2} h^{-1}). (b) Fouling by a protein solution (1000 ppm bovine serum albumin (BSA), 10 mM $CaCl_2$, pH = 6.3, J_0 = 10.0 L m^{-2} h^{-1}). Initial flux was completely recovered after a simple water rinse.

demonstrated exceptional fouling resistance against a solution containing key foulants in surface water, seawater, and wastewater streams,[48−50] comprising humic acid, sodium alginate, and $CaCl_2$ (Figure 5a). The membrane exhibited only minor flux decline during the experiment, likely due to cake deposition. Flux recovery was complete after a simple water rinse, demonstrating complete resistance to irreversible fouling. NF90, a commercial PA-TFC membrane that was tested as a control, demonstrated greater flux decline during the fouling experiment and suffered from irreversible flux loss.

ZAC-X also demonstrated excellent resistance to fouling by a solution of bovine serum albumin (BSA) and 10 mM $CaCl_2$, a protein system known for its high fouling propensity (Figure 5b). We observed minimal flux decline and only 4% irreversible flux loss, consistent with previous studies of sulfobetaine-based r-ZAC membranes.[23,27] NP030, a commer-

https://doi.org/10.1021/acs.chemmater.1c00374
Chem. Mater. 2021, 33, 4408−4416

cial PES-TFC NF membrane that was tested as a control, suffered 45% irreversible flux loss. Collectively, these results illustrate that the exceptional fouling resistance of r-ZAC membranes[22,23,27,28] is not compromised when the nanochannel diameter is reduced to <1.0 nm. Future work will examine if cross-linked r-ZAC membranes also demonstrate the pH and chlorine stability of previous r-ZAC membranes, as well as temperature stability.

Selectivity of Highly Cross-Linked Membranes. The most highly cross-linked membranes, termed ZAC-X (Figures 4 and 5), exhibited extremely small, monodisperse pores (Figure 4b). We observed a >99% retention of sucrose (Figure 4b and 4d) and riboflavin (Figures S7 and S8), ~1 nm neutral solutes that freely pass through advanced BCP membranes designed for small molecule retention[20] and molecular separations.[17] We estimate that ZAC-X possesses a uniform pore size of 0.94 nm based on a fit to the Donnan Steric Pore Model[46] (Figure 4b, eqs S5−S10, Table S3).

The subnanometer effective pore size suggests that ZAC-X can exhibit high selectivity between mono- and divalent ions, because the hydrated diameters of some divalent ions (SO_4^{2-} and Mg^{2+}) are in this size range whereas Na^+ and Cl^- are smaller.[51] Such membranes are extremely valuable for energy-efficient removal of divalent ions from saline solutions with applications in water softening,[4] oil recovery,[52] and the chlor−alkali process.[53] For example, offshore oil production rigs require billions of gallons per day of treated water for enhanced oil recovery.[54] They need to further manage large amounts of produced water recovered along with oil and gas, treating them to sufficient quality for either discharge or reuse.[54] Sulfate ions are undesired in these fluids due to their potential for scaling and due to the presence of sulfate-reducing bacteria that convert it to toxic, corrosive H_2S down many bore holes.[55] While RO and NF membranes are capable of high sulfate removal, they also reject Cl^-, present in much higher concentrations in seawater and frac water used as feeds. This results in high osmotic pressure differences that necessitate high-pressure operation and energy-intensive processes.[52] A membrane that selectively rejects sulfate while allowing the passage of monovalent ions would enable lower pressure, more energy-efficient operation.

To investigate the ion selectivity, we first measured the rejection of various salts. We filtered 20 mM solutions at a consistent flux (6.3−6.9 L m^{-2} h^{-1}) through ZAC-X and a state-of-the-art commercial NF membrane, NF90 (Figure 6a). ZAC-X exhibited a 99.4% rejection of Na_2SO_4 and $MgSO_4$, higher than NF90 (98.8% for Na_2SO_4, 99.2% for $MgSO_4$). Its rejection of chloride salts was lower than that of NF90. This illustrates that ZAC-X has superior selectivity, effectively sieving divalent ions while passing monovalent ions. Low NaCl retention significantly decreases the osmotic pressure difference during operation, enabling lower transmembrane pressures.

For the single-salt filtration experiments (Figure 6a), ZAC-X achieved $S(NaCl/Na_2SO_4)$ = 101. This selectivity surpasses that of nearly every filtration membrane reported to date, including state-of-the-art polyamide TFCs[31,32] and TFNs[9−12] (Figure 1b). Other self-assembled copolymer membranes[29,30] show comparatively negligible Cl^-/SO_4^{2-} selectivity (Figure 1b), further distinguishing the performance of cross-linked r-ZAC membranes. This precise Cl^-/SO_4^{2-} separation was enabled by the exceptionally small nanopores obtained using our novel cross-linking approach. Interestingly, ZAC-X

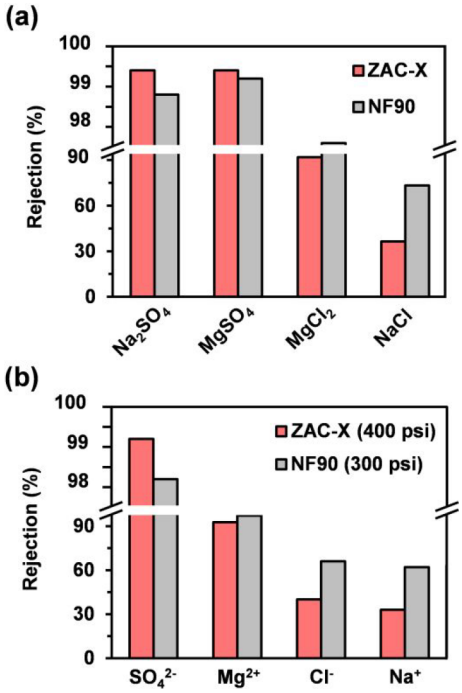

Figure 6. (a) Rejection of single salts (20 mM) by ZAC-X and NF90. Operating flux was 6.3−6.9 L m^{-2} h^{-1}. (b) Rejection of various ions from artificial seawater by ZAC-X and NF90. Composition was C_{SO4} = 28.2 mmol/kg, C_{Mg} = 63.1 mmol/kg, C_{Cl} = 549 mmol/kg, and C_{Na} = 479 mmol/kg. Operating flux was 6 L m^{-2} h^{-1}.

demonstrated far lower selectivity toward cations (e.g., $S(NaCl/MgCl_2)$ = 7.9). While the reason for this is presently unclear, we suspect that specific zwitterion−ion interactions play a crucial role in determining the salt selectivity. Uncovering the exact mechanism for salt permeation and selectivity will be the subject of future work.

While these results are promising, ion retention in complex, realistic feeds often differs from measurements with dilute, single-solute solutions.[29] We therefore challenged ZAC-X with artificial seawater, a highly saline mixture containing appropriate amounts of Na^+, Mg^{2+}, Cl^-, and SO_4^{2-}, and measured the retention of each ion at the same water flux used for the single-salt solutions. The rejection of each ion by ZAC-X closely matched the rejections obtained for the single-salt solutions (Figure 6b). ZAC-X achieved $S(Cl^-/SO_4^{2-})$ = 75 with the artificial seawater, confirming that cross-linked r-ZAC membranes can perform highly selective separations with challenging and complex feedstocks (Figure 1b). This selectivity is ideally suited for offshore oil drilling applications, where the removal of sulfate from injected seawater is crucial to prevent scaling and H_2S production.[52,54] In comparison, NF90 showed only $S(Cl^-/SO_4^{2-})$ = 18 due to its lower retention of SO_4^{2-} and higher retention of Cl^-.

Mono/divalent ion selectivity is crucial in determining the operating transmembrane pressure because any salt rejection contributes to the total osmotic pressure difference the separation system has to overcome.[1] Therefore, the unnecessary removal of ions leads to the need to operate at higher pressure differences, thus adding to energy costs. This is especially important for applications involving saline feedstocks, such as the removal of sulfate from seawater for underground injection for offshore enhanced oil recovery and drilling.[52] Therefore, lower NaCl rejection and higher Cl^-/

https://doi.org/10.1021/acs.chemmater.1c00374
Chem. Mater. 2021, 33, 4408−4416

SO_4^{2-} selectivity can decrease the significance of pure water permeance in achieving sufficiently high flux during operation. This was demonstrated in our experiments. While filtering artificial seawater, the effective osmotic pressure difference during this experiment for ZAC-X was calculated to be ∼170 psi. This value was around 270−290 psi for NF90 due to the higher NaCl rejection (eqs S15 and S16, Table S4). As a result, even though the permeance of ZAC-X (0.40 L m^{-2} h^{-1} bar^{-1}) was a small fraction of that of NF90 (7.0 L m^{-2} h^{-1} bar^{-1}), the two membranes required relatively and unexpectedly similar pressures to filter artificial seawater at 6 L m^{-2} h^{-1}, within 33% of each other (400 psi for ZAC-X and 300 psi for NF90). This outcome underscores the importance of developing membranes with advanced selectivity.[1,56] Improved manufacturing methods can likely improve the pure water permeance of r-ZAC membranes, further closing this gap. As mentioned above, for instance, previous work has shown that the use of ionic liquid additives in r-ZAC coating solutions can boost pure water permeances by up to 50 times.[40] Electrospraying the r-ZAC can also lead to major improvements in water permeance by forming thinner selective layers.[41] Such a processing improvement could potentially enable ZAC-X membranes to operate at lower pressure differences than commercial membranes. This effect is likely to be further compounded by the higher fouling resistance of ZAC-X, leading to significant energy and cost savings upon optimization of this membrane system.

CONCLUSIONS

This work demonstrates novel self-assembled zwitterionic membranes with tunable selectivity, subnanometer nanochannels, and unmatched fouling resistance accessed by a new and scalable cross-linking approach that controls the aqueous swelling of the nanopores. It is, to our knowledge, the first demonstration of the use of cross-linking to tune the pore size of self-assembled copolymer membranes, thus enabling the design of nanostructured membranes with tailored selectivity in a novel manner. Highly cross-linked membranes prepared using this method demonstrated excellent retention of divalent ions and an effective pore size ≈ 0.9 nm, smaller than that of any other self-assembled copolymer membrane. The membranes achieved $S(NaCl/Na_2SO_4)$ = 101 for single-salt solutions and $S(Cl^-/SO_4^{2-})$ = 75 for artificial seawater, outperforming state-of-the-art membrane technologies. They also completely resisted irreversible fouling by two critical foulant families, promising reliable operation even with high-fouling feeds. These findings demonstrate the potential for cross-linked r-ZAC membranes to perform a wide range of separations, including sulfate removal from seawater for oil drilling, water softening, ion separations for resource recovery, and removal of micropollutants from drinking water.

EXPERIMENTAL SECTION

Copolymer Synthesis. We first dissolved 40 g of SBMA, 60 g of AMA, and 1.55 mmol of ethyl α-bromoisobutyrate in 700 mL of 50:50 methanol:acetonitrile. After purging the mixture with nitrogen, we initiated ARGET-ATRP by adding 0.0614 mmol of $CuBr_2$, 0.619 mmol of ascorbic acid, and 0.619 mmol of *N*,*N*,*N*′,*N*″,*N*″-pentamethyldiethylenetriamine (PMDETA) dissolved in 50.1 mL of 50:50 methanol:acetonitrile. The reaction was conducted for 20 h at room temperature and terminated by exposure to air. The copolymer was precipitated in 2400 mL of 3:5 ethanol:hexane, redissolved and reprecipitated several times using the same solvent system, and washed for several days in hexane. It was finally dried under vacuum at room temperature for several days.

Copolymer Characterization. Copolymer composition was measured by ^{1}H NMR spectroscopy (Bruker Avance III 500 MHz). Samples were dissolved in deuterated dimethyl sulfoxide (d_6-DMSO) and scanned 32 times using a 10 s relaxation delay.

DLS was performed using a Nano Brook 90Plus PALS particle sizer (Brookhaven Instruments) equipped with a He−Ne laser operated at 659 nm and with a 1 mm entrance aperture at 25 °C and 90° angle. The copolymer was dissolved in either TFE or DMSO at 2 mg/mL and passed through a 0.45 μm Teflon syringe filter prior to analysis.

DSC was performed using a TA Q100 series calorimeter (TA Instruments) equipped with a refrigerated cooling system and purged with N_2. We sealed 3−5 mg of copolymer in aluminum pans, equilibrated at 120 °C for 15 min, cooled to −80 °C, and performed two heating/cooling cycles where we ramped from −80 to 180 °C at 30 °C/min. The T_g was taken as the midpoint of the baseline shift from the second run.

TEM was performed using a Hitachi 7800 transmission electron microscope operated in bright-field mode at 100 keV. Uncross-linked copolymer films were prepared by evaporating the solvent from a copolymer/TFE solution in a Teflon dish. Zwitterionic domains were positively stained by immersing the films in a 2 wt % solution of $CuCl_2$ overnight. The stained films were then embedded in an epoxy resin, sectioned to 50 nm using an ultramicrotome, and transferred to copper grids. The imaging was performed by Dr. Nicki Watson at the Harvard Center for Nanoscale Systems (CNS). TEM images were analyzed using ImageJ software.

ATR-FTIR spectroscopy was performed using an FT/IR-6200 spectrophotometer (JASCO Corp) equipped with a ZnSe crystal. ATR-FTIR spectra (4000−600 cm^{-1}, 4 cm^{-1} resolution, 64 scans) were collected using ∼50 μm copolymer films prepared by drying a 3 wt % solution of P(AMA-*r*-SBMA) in TFE on a glass plate and then cross-linking as described below.

Water uptake measurements were performed using a ZETA-20 optical profilometer (KLA-Tencor Co.) equipped with a 100× lens. Uptake was determined by measuring the wet and dry thickness of ∼2 μm copolymer films prepared by spin casting a 3 wt % solution of P(AMA-*r*-SBMA) in TFE onto silicon wafers (Figure S3, eq S2).

Membrane Preparation/Characterization. A 3 wt % solution of P(AMA-*r*-SBMA) in TFE was cast onto a commercial UF membrane (PS35, Solecta) support using a wire-wound metering rod (Gardco, #10). Immediately after casting, we used a heat gun (Sparkfun Electronics) to blow hot air across the surface, thereby accelerating the rate of solvent evaporation. This step was performed to simulate the casting conditions of certain commercial coating lines. Membranes were stored in deionized water for several hours prior to use.

The TFC membrane morphology was characterized using a Zeiss Supra55 VP FESEM. Membranes were freeze fractured in liquid nitrogen, mounted, and sputter coated with Au/Pd. To determine if the selective layer became insoluble in TFE upon cross-linking, membranes were immersed in TFE for >1 h prior to freeze fracturing.

Cross-Linking. Coated membranes or P(AMA-*r*-SBMA) films were first equilibrated with a 0.30−4.0 w/v % solution of photoinitiator (2-hydroxy-2-methylpropiophenone) in isopropyl alcohol for at least 20 min. To cross-link, the membranes or films were then sandwiched between two glass plates and exposed to UV light for 5−20 min. The membranes or films were finally transferred to isopropanol for 20 min and stored in deionized water for several hours prior to use.

Membrane Testing. Filtration experiments were performed on 4.7 cm diameter membrane disks using stainless steel cells (HP 4750, Sterlitech) stirred at 1000 rpm and pressurized to 20−400 psi. Rejection (R) was determined by $R = (1 - C_P/C_F) \times 100\%$, where C_P and C_F are the permeate and feed concentrations, respectively. For rejection measurements, we loaded 125 mL of feed solution, filtered >6 mL, and then collected the next permeate fraction for analysis. Solute concentration was measured using a conductivity meter (high range, VWR), COD kits (TNT 821, Hach), Sulfaver kits (Hach),

https://doi.org/10.1021/acs.chemmater.1c00374
Chem. Mater. 2021, 33, 4408−4416

water hardness kits (TNT 869, Hach), or a UV−vis spectrometer (Genesys10, ThermoScientific). Selectivity (S) was determined by $S(i/j) = (100 - R_i)/(100 - R_j)$. For the fouling experiments, we monitored flux (J) normalized by initial flux (J_0) during the 12 h fouling period. Membranes were gently rinsed with water before measuring the final flux. The initial and final fluxes were determined using the appropriate background electrolyte solution.

■ ASSOCIATED CONTENT

Supporting Information

The Supporting Information is available free of charge at https://pubs.acs.org/doi/10.1021/acs.chemmater.1c00374.

Materials, Cl^-/SO_4^{2-} selectivity comparison, polymer synthesis, copolymer ^1H NMR spectra, hydrodynamic diameter and molecular weight, Fox equation calculations, FFT, water uptake, setup for membrane casting and cross-linking, Donnan Steric Pore Model, neutral solute rejections, details of artificial seawater permeate analysis, osmotic pressure calculation, and details of fouling experiments (PDF)

■ AUTHOR INFORMATION

Corresponding Author

Ayse Asatekin − *Department of Chemical and Biological Engineering, Tufts University, Medford, Massachusetts 02155, United States;* orcid.org/0000-0002-4704-1542; Email: ayse.asatekin@tufts.edu

Author

Samuel J. Lounder − *Department of Chemical and Biological Engineering, Tufts University, Medford, Massachusetts 02155, United States*

Complete contact information is available at: https://pubs.acs.org/10.1021/acs.chemmater.1c00374

Notes

The authors declare the following competing financial interest(s): Ayse Asatekin owns a minor equity in and serves as the Senior Scientific Advisor of ZwitterCo. Inc., which was the lead institution in the NSF grant IIP-1843847 that partially funded this work. ZwitterCo also holds a license from Tufts University to commercialize the technology described in this manuscript. Samuel J. Lounder declares no conflict of interest.

■ ACKNOWLEDGMENTS

We gratefully acknowledge financial support from the National Science Foundation (NSF) under grant nos. CBET-1553661 and IIP-1843847 led by ZwitterCo, Inc. We thank Dr. Nicki Watson at the Harvard Center for Nanoscale Systems (CNS), for collecting the TEM images. The Center for Nanoscale Systems (CNS), a member of the National Nanotechnology Coordinated Infrastructure Network (NNCI), was supported by the National Science Foundation under NSF award no. 1541959. FESEM images were collected by Microvision Laboratories, Inc. We thank Solecta membranes for donating PS35 support membranes. A.A. thanks Chris Drover for helpful conversations regarding the potential commercial applications and scale-up processes for this technology. S.J.L. thanks Hannah Drew and Jordan Houdeshell for helpful discussions.

■ REFERENCES

(1) Werber, J. R.; Deshmukh, A.; Elimelech, M. The Critical Need for Increased Selectivity, Not Increased Water Permeability, for Desalination Membranes. *Environ. Sci. Technol. Lett.* **2016**, *3* (4), 112−120.

(2) Yao, Y.; Zhang, P.; Jiang, C.; DuChanois, R. M.; Zhang, X.; Elimelech, M. High performance polyester reverse osmosis desalination membrane with chlorine resistance. *Nature Sustainability* **2021**, *4*, 138−146.

(3) Mauter, M. S.; Zucker, I.; Perreault, F. o.; Werber, J. R.; Kim, J.-H.; Elimelech, M. The role of nanotechnology in tackling global water challenges. *Nature Sustainability* **2018**, *1* (4), 166−175.

(4) Van der Bruggen, B.; Vandecasteele, C. Removal of pollutants from surface water and groundwater by nanofiltration: overview of possible applications in the drinking water industry. *Environ. Pollut.* **2003**, *122*, 435−445.

(5) Zhang, R.; Liu, Y.; He, M.; Su, Y.; Zhao, X.; Elimelech, M.; Jiang, Z. Antifouling membranes for sustainable water purification: strategies and mechanisms. *Chem. Soc. Rev.* **2016**, *45* (21), 5888−5924.

(6) Werber, J. R.; Osuji, C. O.; Elimelech, M. Materials for next-generation desalination and water purification membranes. *Nat. Rev. Mater.* **2016**, *1*, 16018.

(7) Shannon, M. A.; Bohn, P. W.; Elimelech, M.; Georgiadis, J. G.; Marinas, B. J.; Mayes, A. M. Science and technology for water purification in the coming decades. *Nature* **2008**, *452*, 301−10.

(8) Sadeghi, I.; Kaner, P.; Asatekin, A. Controlling and Expanding the Selectivity of Filtration Membranes †. *Chem. Mater.* **2018**, *30* (21), 7328−7354.

(9) Liu, T.-Y.; Yuan, H.-G.; Li, Q.; Tang, Y.-H.; Zhang, Q.; Qian, W.; Van der Bruggen, B.; Wang, X. Ion-Responsive Channels of ZwitterionCarbon Nanotube Membrane for Rapid Water Permeation and Ultrahigh Mono-/Multivalent Ion Selectivity. *ACS Nano* **2015**, *9*, 7488−7496.

(10) Wang, J.; Wang, Y.; Zhu, J.; Zhang, Y.; Liu, J.; Van der Bruggen, B. Construction of TiO2@graphene oxide incorporated antifouling nanofiltration membrane with elevated filtration performance. *J. Membr. Sci.* **2017**, *533*, 279−288.

(11) Zhu, J.; Hou, J.; Yuan, S.; Zhao, Y.; Li, Y.; Zhang, R.; Tian, M.; Li, J.; Wang, J.; Van der Bruggen, B. MOF-positioned polyamide membranes with a fishnet-like structure for elevated nanofiltration performance. *J. Mater. Chem. A* **2019**, *7* (27), 16313−16322.

(12) Ji, Y.-L.; An, Q.-F.; Guo, Y.-S.; Hung, W.-S.; Lee, K.-R.; Gao, C.-J. Bio-inspired fabrication of high perm-selectivity and anti-fouling membranes based on zwitterionic polyelectrolyte nanoparticles. *J. Mater. Chem. A* **2016**, *4* (11), 4224−4231.

(13) Moon, J. D.; Freeman, B. D.; Hawker, C. J.; Segalman, R. A. Can Self-Assembly Address the Permeability/Selectivity Trade-Offs in Polymer Membranes? *Macromolecules* **2020**, *53* (14), 5649−5654.

(14) Asatekin, A.; Vannucci, C. Self-Assembled Polymer Nanostructures for Liquid Filtration Membranes: A Review. *Nanosci. Nanotechnol. Lett.* **2015**, *7* (1), 21−32.

(15) Carter, B. M.; Wiesenauer, B. R.; Hatakeyama, E. S.; Barton, J. L.; Noble, R. D.; Gin, D. L. Glycerol-based bicontinuous cubic lyotropic liquid crystal monomer system for the fabrication of thin-film membranes with uniform nanopores. *Chem. Mater.* **2012**, *24* (21), 4005−4007.

(16) Dischinger, S. M.; Rosenblum, J.; Noble, R. D.; Gin, D. L. Evaluation of a nanoporous lyotropic liquid crystal polymer membrane for the treatment of hydraulic fracturing produced water via cross-flow filtration. *J. Membr. Sci.* **2019**, *592* (March), 117313.

(17) Zhang, Z.; Rahman, M. M.; Abetz, C.; Hohme, A. L.; Sperling, E.; Abetz, V. Chemically Tailored Multifunctional Asymmetric Isoporous Triblock Terpolymer Membranes for Selective Transport. *Adv. Mater.* **2020**, *32* (8), 1907014.

(18) Zhang, Z.; Rahman, M. M.; Abetz, C.; Abetz, V. High-performance asymmetric isoporous nanocomposite membranes with chemically-tailored amphiphilic nanochannels. *J. Mater. Chem. A* **2020**, *8* (19), 9554−9566.

(19) Zhang, Y.; Almodovar-Arbelo, N. E.; Weidman, J. L.; Corti, D. S.; Boudouris, B. W.; Phillip, W. A. Fit-for-purpose block polymer membranes molecularly engineered for water treatment. *npj Clean Water* **2018**, *1* (1), 2.

(20) Zhang, Y.; Mulvenna, R. A.; Qu, S.; Boudouris, B. W.; Phillip, W. Block Polymer Membranes Functionalized with Nanoconfined Polyelectrolyte Brushes Achieve Sub-Nanometer Selectivity. *ACS Macro Lett.* **2017**, *6* (7), 726−732.
(21) Nunes, S. P.; Behzad, A. R.; Hooghan, B.; Sougrat, R.; Karunakaran, M.; Pradeep, N.; Vainio, U.; Peinemann, K. V. Switchable pH-Responsive Polymeric Membranes Prepared via Block Copolymer Micelle Assembly. *ACS Nano* **2011**, *5*, 3516−3522.
(22) Bengani, P.; Kou, Y.; Asatekin, A. Zwitterionic copolymer self-assembly for fouling resistant, high flux membranes with size-based small molecule selectivity. *J. Membr. Sci.* **2015**, *493*, 755−765.
(23) Bengani-Lutz, P.; Converse, E.; Cebe, P.; Asatekin, A. Self-Assembling Zwitterionic Copolymers as Membrane Selective Layers with Excellent Fouling Resistance: Effect of Zwitterion Chemistry. *ACS Appl. Mater. Interfaces* **2017**, *9* (24), 20859−20872.
(24) Ehrmann, M.; Galin, J. C.; Meurer, B. Statistical N-Butyl Acrylate Sulfopropyl Betaine Copolymers 0.3. Domain Size Determination by Solid-State Nmr-Spectroscopy. *Macromolecules* **1993**, *26* (5), 988−993.
(25) Wu, T. Y.; Beyer, F. L.; Brown, R. H.; Moore, R. B.; Long, T. E. Influence of Zwitterions on Thermomechanical Properties and Morphology of Acrylic Copolymers: Implications for Electroactive Applications. *Macromolecules* **2011**, *44* (20), 8056−8063.
(26) Bengani-Lutz, P.; Sadeghi, I.; Lounder, S. J.; Panzer, M. J.; Asatekin, A. High Flux Membranes with Ultrathin Zwitterionic Copolymer Selective Layers with ∼ 1 nm Pores Using an Ionic Liquid Cosolvent. *ACS Applied Polymer Materials* **2019**, *1* (8), 1954−1959.
(27) Bengani-Lutz, P.; Zaf, R. D.; Culfaz-Emecen, P. Z.; Asatekin, A. Extremely fouling resistant zwitterionic copolymer membranes with ∼ 1 nm pore size for treating municipal, oily and textile wastewater streams. *J. Membr. Sci.* **2017**, *543*, 184−194.
(28) Dudchenko, A. V.; Bengani-Lutz, P.; Asatekin, A.; Mauter, M. S. Foulant Adsorption to Heterogeneous Surfaces with Zwitterionic Nanoscale Domains. *ACS Applied Polymer Materials* **2020**, *2* (11), 4709−4718.
(29) Sadeghi, I.; Kronenberg, J.; Asatekin, A. Selective Transport through Membranes with Charged Nanochannels Formed by Scalable Self-Assembly of Random Copolymer Micelles. *ACS Nano* **2018**, *12* (1), 95−108.
(30) Qu, S.; Dilenschneider, T.; Phillip, W. A. Preparation of Chemically-Tailored Copolymer Membranes with Tunable Ion Transport Properties. *ACS Appl. Mater. Interfaces* **2015**, *7* (35), 19746−54.
(31) Liang, Y.; Zhu, Y.; Liu, C.; Lee, K. R.; Hung, W. S.; Wang, Z.; Li, Y.; Elimelech, M.; Jin, J.; Lin, S. Polyamide nanofiltration membrane with highly uniform sub-nanometre pores for sub-1 A precision separation. *Nat. Commun.* **2020**, *11* (1), 2015.
(32) Nanofiltration (NF) Membranes- Flat Sheet Membranes; https://www.sterlitech.com/nanofiltration-nf-membrane.html (accessed Nov 19, 2020).
(33) Hu, M.; Mi, B. Enabling graphene oxide nanosheets as water separation membranes. *Environ. Sci. Technol.* **2013**, *47* (8), 3715−23.
(34) Zhang, M.; Guan, K.; Ji, Y.; Liu, G.; Jin, W.; Xu, N. Controllable ion transport by surface-charged graphene oxide membrane. *Nat. Commun.* **2019**, *10* (1), 1253.
(35) París, R.; De La Fuente, J. L. Bulk atom transfer radical polymerization of allyl methacrylate. *J. Polym. Sci., Part A: Polym. Chem.* **2005**, *43* (11), 2395−2406.
(36) Wang, X.-Y.; Sun, X.-L.; Chen, Z.-H.; Wang, F.; Wang, S. R.; Tang, Y. Highly efficient access to well-defined linear polymers with substantial vinyl pendants via ATRP of divinyl monomers. *Polym. Chem.* **2018**, *9*, 4309−4315.
(37) París, R.; De la Fuente, J. L. Glass transition temperature of allyl methacrylate-n-butyl acrylate gradient copolymers in dependence on chemical composition and molecular weight. *J. Polym. Sci., Part B: Polym. Phys.* **2007**, *45* (14), 1845−1855.
(38) Ehrmann, M.; Mathis, A.; Meurer, B.; Scheer, M.; Galin, J. C. Statistical n-Butyl Acrylate-(Sulfopropyl) ammonium Betaine Copolymers. 2. Structural Studies. *Macromolecules* **1992**, *25* (8), 2253−2261.
(39) Fujita, T.; Chen, M. W. Characteristic Length Scale of Bicontinuous Nanoporous Structure by Fast Fourier Transform. *Jpn. J. Appl. Phys.* **2008**, *47*, 1161−1163.
(40) Bengani-Lutz, P.; Sadeghi, I.; Lounder, S. J.; Panzer, M. J.; Asatekin, A. High Flux Membranes with Ultrathin Zwitterionic Copolymer Selective Layers with ∼ 1 nm Pores Using an Ionic Liquid Cosolvent. *ACS Applied Polymer Materials* **2019**, *1* (8), 1954−1959.
(41) Qian, X.; Ravindran, T.; Lounder, S. J.; Asatekin, A.; McCutcheon, J. R. Printing zwitterionic self-assembled thin film composite membranes: Tuning thickness leads to remarkable permeability for nanofiltration. *J. Membr. Sci.* **2021**, 119428.
(42) Vardareli, T. K.; Keskin, S.; Usanmaz, A. Synthesis and Characterization of Poly(allyl methacrylate) Obtained by Free Radical Initiator. *J. Macromol. Sci., Part A: Pure Appl.Chem.* **2008**, *45* (4), 302−311.
(43) Brown, R. H.; Duncan, A. J.; Choi, J. H.; Park, J. K.; Wu, T.; Leo, D. J.; Winey, K. I.; Moore, R. B.; Long, T. E. Effect of ionic liquid on mechanical properties and morphology of zwitterionic copolymer membranes. *Macromolecules* **2010**, *43* (2), 790−796.
(44) Galin, M.; Mathis, A.; Galin, J. C. Statistical n-Butyl Acrylate-(Sulfopropyl)ammonium Betaine Copolymers. 5. Plasticization Studies. *Macromolecules* **1993**, *26* (18), 4919−4927.
(45) Geise, G. M.; Paul, D. R.; Freeman, B. D. Fundamental water and salt transport properties of polymeric materials. *Prog. Polym. Sci.* **2014**, *39* (1), 1−42.
(46) Bowen, W. R.; Mohammad, A. W. Diafiltration by nanofiltration: Prediction and optimization. *AIChE J.* **1998**, *44* (8), 1799−1812.
(47) Greenlee, L. F.; Lawler, D. F.; Freeman, B. D.; Marrot, B.; Moulin, P. Reverse osmosis desalination: water sources, technology, and today's challenges. *Water Res.* **2009**, *43* (9), 2317−2348.
(48) Jarusutthirak, C.; Amy, G.; Croue, J. P. Fouling characteristics of wastewater effluent organic matter (EfOM) isolates on NF and UF membranes. *Desalination* **2002**, *145* (1−3), 247−255.
(49) Manttari, M.; Puro, L.; Nuortila-Jokinen, J.; Nystrom, M. Fouling effects of polysaccharides and humic acid in nanofiltration. *J. Membr. Sci.* **2000**, *165* (1), 1−17.
(50) Li, Q. L.; Elimelech, M. Organic fouling and chemical cleaning of nanofiltration membranes: Measurements and mechanisms. *Environ. Sci. Technol.* **2004**, *38* (17), 4683−4693.
(51) Nightingale, E. R. Phenomenological theory of ion solvation. Effective radii of hydrated ions. *J. Phys. Chem.* **1959**, *63* (9), 1381−1387.
(52) Bader, M. S. H. Sulfate removal technologies for oil fields seawater injection operations. *J. Pet. Sci. Eng.* **2007**, *55* (1), 93−110.
(53) Valderrama, C. Membranes in the Chlor-Alkali Industry. In *Encyclopedia of Membranes*; Drioli, E., Giorno, L., Eds.; Springer Berlin Heidelberg: Berlin, Heidelberg, 2015; pp 1−5.
(54) Fakhru'l-Razi, A.; Pendashteh, A.; Abdullah, L. C.; Biak, D. R.; Madaeni, S. S.; Abidin, Z. Z. Review of technologies for oil and gas produced water treatment. *J. Hazard. Mater.* **2009**, *170* (2−3), 530−51.
(55) Johnson, R. J.; Folwell, B. D.; Wirekoh, A.; Frenzel, M.; Skovhus, T. L. Reservoir Souring - Latest developments for application and mitigation. *J. Biotechnol.* **2017**, *256*, 57−67.
(56) Gao, F.; Hunter, A.; Qu, S.; Hoffman, J. R.; Gao, P.; Phillip, W. A. Interfacial Junctions Control Electrolyte Transport through Charge-Patterned Membranes. *ACS Nano* **2019**, *13* (7), 7655−7664.

https://doi.org/10.1021/acs.chemmater.1c00374
Chem. Mater. 2021, 33, 4408−4416